

Convergence Analysis of Sparsified Asynchronous SGD

Rosa Candela, Giulio Franzese, Maurizio Filippone, and Pietro Michiardi

Abstract. Large scale machine learning is increasingly relying on distributed optimization, whereby several machines contribute to the training process of a statistical model. In this work we study the performance of asynchronous, distributed settings, when applying sparsification, a technique used to reduce communication overheads. In particular, for the first time in an asynchronous, non-convex setting, we theoretically prove that, in presence of staleness, sparsification does not harm SGD performance: the ergodic convergence rate matches the known result of standard SGD, that is $\mathcal{O}(1/\sqrt{T})$. We also carry out an empirical study to complement our theory, and confirm that the effects of sparsification on the convergence rate are negligible, when compared to “vanilla” SGD, even in the challenging scenario of an asynchronous, distributed system.

Keywords: Stochastic Optimization · Asynchronous · Sparsification.

1 Introduction

The analysis of Stochastic Gradient Descent (SGD) [31] and its variants has received a lot of attention recently, due to its popularity as an optimization algorithm in machine learning; see [8] for an overview. SGD addresses the computational bottleneck of gradient descent by relying on stochastic gradients, which are cheaper to compute than full gradients. SGD trades a larger number of iterations to converge for a cheaper cost per iteration. The *mini-batch* variant of SGD allows one to control the number and the cost per iteration, making it the preferred choice for optimization in deep learning [7,8].

We consider the problem of optimizing the d -dimensional parameter vector $\mathbf{x} \in \mathbb{R}^d$ of a model and its associated finite-sum *non-convex* loss function $f(\mathbf{x}) = \frac{1}{n} \sum_{i=1}^n f(\mathbf{x}, i)$, where $f(\mathbf{x}, i)$, $i = 1, \dots, n$ is the loss function for a single training sample i . SGD iterations have the following form:

$$\mathbf{x}_{t+1} = \mathbf{x}_t - \eta_t \mathbf{g}(\mathbf{x}_t, i),$$

where $\mathbf{x}_t, \mathbf{x}_{t+1} \in \mathbb{R}^d$ are the model iterates, $\eta_t > 0$ is the learning rate/step size and $\mathbf{g}(\mathbf{x}_t, i) = \nabla f(\mathbf{x}_t, i)$ is a stochastic gradient.

In this work, we are interested in the increasingly popular distributed setting, whereby SGD runs across several machines, which contribute to the model updates \mathbf{x}_{t+1} by computing stochastic gradients of the loss using locally available training data [14,20,10,23,21]. The analysis of the convergence behavior of

SGD, both in synchronous [9,43,8] and asynchronous [30,13,24,27,8] settings has been widely studied in the literature. In this work, we focus on the asynchronous setting, which is particularly challenging because distributed workers might produce gradient updates for a loss computed on *stale* versions of the current model iterates [20,12,25,16,11].

In this context, communication overheads have been considered as a key issue to address, and a large number of works have been proposed to mitigate such overheads [37,42,39,3,40,2,1]. In particular, sparsification methods [35,4,39] have achieved remarkable results, albeit for synchronous setups. The key idea is to apply smaller and more efficient gradient updates, by applying a sparsification operator to the stochastic gradient, which results in updates of size $k \ll d$.

In this work, we fill the gap in the literature and study sparsification methods in *asynchronous settings*. For the first time, we provide a concise and simple convergence rate analysis when the joint effects of sparsification and asynchrony are taken into account, and show that sparsified SGD converges at the same rate of standard SGD. Our empirical analysis of sparsified SGD complements our theory. We consider several delay distributions and show that, in practice, applying sparsification does not harm SGD performance. These results carry over when the system scales out, which is a truly desirable property.

1.1 Related work

The analysis of SGD [31] and its convergence properties has recently attracted a lot of attention, especially in the field of machine learning [8,29], where SGD is considered the workhorse optimization method. Large scale models and massive datasets have motivated researchers to focus on distributed machine learning, whereby multiple machines compute stochastic gradients using partitions of the dataset and a parameter server maintains a globally shared model.

Asynchronous systems [30,14,23,10] provide fast model updates, but the use of stale parameters might affect convergence speed. One way to reduce the staleness effect is to give a smaller weight to stale updates. In [21,12] gradient contributions are dampened through a dynamic learning rate. Stale-synchronous parallel (SSP) models [20,12] limit instead the maximum staleness, discarding updates that are too “old”. Interestingly, the work in [28], suggests to view staleness as a form of implicit momentum, and study, under a simple model, how to adjust explicit, algorithmic momentum to counterbalance the effects of staleness.

Synchronous systems [9] guarantee higher statistical efficiency, but the presence of stragglers slows down the learning algorithm. One solution is provided by the so called local SGD models [25,37,42], which reduce the synchronization frequency by allowing nodes to compute local model parameters, which are averaged in a global model update. A second family of approaches seeks to improve synchronous systems by reducing the cost of communicating gradients upon every iteration. Quantization techniques reduce the number of bits to represent the gradients before communication [33,3,40], sparsification methods select a subset of the gradient components to communicate [2,1,38,35,4,26], and loss-

less methods use large mini-batches to increase the computation-communication ratio [19,41].

Our work, along the lines of [24,4], argues instead that staleness vanishes, asymptotically. Similarly, recent work [36] uses an elegant analysis technique to study the role of stale gradient updates and sparsification, albeit their effects are considered in isolation. In this work, instead, we provide a concise and simple convergence rate analysis for the joint effects of sparsification and staleness.

1.2 Contributions

We study finite-sum non-convex optimization of loss functions of the form $f(\mathbf{x}) : \mathbb{R}^d \rightarrow \mathbb{R}$, and assume that f is continuously differentiable and bounded below, that $\nabla f(\mathbf{x})$ is L -Lipschitz smooth, that the variance of stochastic gradients is bounded, and that the staleness induced by asynchrony is also bounded. We analyze a mini-batch asynchronous SGD algorithm and apply a sparsification operator $\Phi_k[\mathbf{g}(\mathbf{x}_{\tau_t}, \xi_t)]$ with $k \ll d$, which can be coupled with an error correction technique, often called *memory* [35].

We prove ergodic convergence of the gradient of $f(\mathbf{x})$, for an appropriately chosen learning rate. In particular, we focus on memory-less variants, which are simpler to analyze, and show that asynchronous sparsified SGD converges at the same rate as standard SGD.

In this paper, the main theoretical contribution is as follows. Let the sparsification coefficient be $\rho = k/d$. Then, it holds that:

$$\min_{0 \leq t \leq T} \mathbb{E} \left[\|\nabla f(\mathbf{x}_t)\|^2 \right] \leq \frac{\left(\sum_{t=0}^{T-1} \left(\frac{\eta_t^2 L}{2} \sigma^2 \right) \right) + \Lambda + C}{\sum_{t=0}^{T-1} \left(\eta_t \rho \mu - \frac{\eta_t^2 L}{2} \right)},$$

where $\Lambda = f(\mathbf{x}_0) - \inf_{\mathbf{x}} f(\mathbf{x})$ and C, μ are finite positive constants (whose role will be clarified later). In particular for a suitable constant learning rate $\eta_t = \eta = \frac{\rho \mu}{L \sqrt{T}}$ we can derive as a corollary that:

$$\min_{0 \leq t \leq T} \mathbb{E} \left[\|\nabla f(\mathbf{x}_t)\|^2 \right] \leq \left(\frac{\sigma^2}{2} + \frac{(\Lambda + C)L}{(\rho \mu)^2} \right) \frac{1}{\sqrt{T}},$$

up to a negligible approximation for large T (details in the supplement).

We define sparsified SGD formally in Section 2, both in its memory and memory-less variants, and outline our proof for the memory-less case in Section 3.1. In Section 4 we provide an empirical study of the convergence behavior of the two variants of sparsified SGD, using simple and deep convolutional networks for image classification tasks. Our experiments show that sparsification does not harm SGD performance, even in the challenging scenario of an asynchronous, distributed system. Although we do not provide convergence guarantees for sparsified SGD with memory, our empirical results indicate that error correction dramatically improves the convergence properties of the algorithm.

2 Sparsified Asynchronous SGD

In this Section we define two variants of sparsified SGD algorithms, with and without error correction, and emphasize the role of model staleness induced by the asynchronous setup we consider.

The standard way to scale SGD to multiple computing nodes is via *data-parallelism*: a set of worker machines have access to the n training samples through a distributed filesystem. Workers process samples concurrently: each node receives a copy of the parameter vector \mathbf{x}_t , and computes stochastic gradients locally. Then, they send their gradients to a parameter server (PS). Upon receiving a gradient from a worker, the PS updates the model by producing a new iterate \mathbf{x}_{t+1} .

Due to asynchrony, a computing node may use a *stale* version of the parameter vector: a worker may compute the gradient of $f(\mathbf{x}_{\tau_t})$, $\tau_t \leq t$. We call τ_t the *staleness of a gradient update*. As stated more formally in Section 3, in this work we assume **bounded staleness**, which is realistic in the setup we consider. Other works, e.g. that consider Byzantine attackers [12], drop this assumption.

Gradient sparsification. A variety of compression [5,6], quantization [1,3] and sparsification [4,35] operators have been considered in the literature. Here we use sparsification, defined as follows:

Definition 1. Given a vector $\mathbf{u} \in \mathbb{R}^d$, a parameter $1 \leq k \leq d$, the operator $\Phi_k(\mathbf{u}) : \mathbb{R}^d \rightarrow \mathbb{R}^d$ is defined as:

$$(\Phi_k(\mathbf{u}))_i = \begin{cases} (\mathbf{u})_{\pi(i)}, & \text{if } i \leq k, \\ 0, & \text{otherwise} \end{cases}$$

where π is a permutation of the indices $\{1, \dots, d\}$ such that $(|\mathbf{u}|)_{\pi(i)} \geq (|\mathbf{u}|)_{\pi(i+1)}$, $\forall i \in 1, \dots, d$.

Essentially, $\Phi_k(\cdot)$ sorts vector elements by their magnitude, and keeps only the top- k . A key property of the operator we consider is called the k -contraction property [35], which we use in our convergence proofs.

Definition 2. For a parameter $1 \leq k \leq d$, a k -contraction operator $\Phi_k(\mathbf{u}) : \mathbb{R}^d \rightarrow \mathbb{R}^d$ satisfies the following contraction property:

$$\mathbb{E} \|\mathbf{u} - \Phi_k(\mathbf{u})\|^2 \leq \left(1 - \frac{k}{d}\right) \|\mathbf{u}\|^2.$$

Both the top- k operator we consider, and randomized variants, satisfy the k -contraction property [4,35]. Next, we state a Lemma that we will use for our convergence rate results.

Lemma 1. Given a vector $\mathbf{u} \in \mathbb{R}^d$, a parameter $1 \leq k \leq d$, and the top- k operator $\Phi_k(\mathbf{u}) : \mathbb{R}^d \rightarrow \mathbb{R}^d$ introduced in Definition 1, we have that:

$$\|\Phi_k(\mathbf{u})\|^2 \geq \frac{k}{d} \|\mathbf{u}\|^2.$$

The proof of Lemma 1 uses the k -contraction property in Definition 2, as shown in Appendix A.1.

Memory and memory-less sparsified asynchronous SGD. We define two variants of sparsified SGD: the first uses sparsified stochastic gradient updates directly, whereas the second uses an error correction technique which accumulates information suppressed by sparsification. Since we consider an asynchronous, *mini-batch* version of SGD, additional specifications are in order.

Definition 3. *Given n training samples, let ξ_t be a set of indices sampled uniformly at random from $\{1, \dots, n\}$, with cardinality $|\xi_t|$. Let τ_t be the bounded staleness induced by the asynchronous setup, with respect to the current iterate t . That is, $t - S \leq \tau_t \leq t$. A stale, mini-batch stochastic gradient is defined as:*

$$\mathbf{g}(\mathbf{x}_{\tau_t}, \xi_t) = \frac{1}{|\xi_t|} \sum_{i \in \xi_t} \nabla f(\mathbf{x}_{\tau_t}, i).$$

Memory-less sparsified SGD. Given the operator $\Phi_k(\cdot)$, the memory-less, asynchronous sparsified SGD algorithm amounts to the following:

$$\mathbf{x}_{t+1} = \mathbf{x}_t - \eta_t \Phi_k(\mathbf{g}(\mathbf{x}_{\tau_t}, \xi_t)),$$

where $\{\eta_t\}_{t \geq 0}$ denotes a sequence of learning rates.

Sparsified SGD with memory. Given the operator $\Phi_k(\cdot)$, the asynchronous sparsified SGD with memory algorithm is defined as:

$$\begin{aligned} \mathbf{x}_{t+1} &= \mathbf{x}_t - \eta_t \Phi_k(\mathbf{m}_t + \mathbf{g}(\mathbf{x}_{\tau_t}, \xi_t)), \\ \mathbf{m}_{t+1} &= \mathbf{m}_t + \mathbf{g}(\mathbf{x}_{\tau_t}, \xi_t) - \Phi_k(\mathbf{m}_t + \mathbf{g}(\mathbf{x}_{\tau_t}, \xi_t)), \end{aligned}$$

where $\{\eta_t\}_{t \geq 0}$ denotes a sequence of learning rates, and \mathbf{m}_t represents the memory vector that accumulates the elements of the stochastic gradient that have been suppressed by the operator $\Phi_k(\cdot)$.

3 Ergodic convergence

In this work, we focus on the memory-less variant of SGD, and we study its convergence properties. The convergence of sparsified SGD with memory has been studied for both strongly convex [35,4] and non-convex objectives [4], but only in the synchronous case. Nevertheless, in our empirical study, we compare both variants, and verify that the one with memory considerably benefits from error correction, as expected [35]. Before proceeding with the statement of the main theorem, we formalize our assumptions.

Assumption 1 $f(\mathbf{x})$ is continuously differentiable and bounded below:

$$\inf_x f(\mathbf{x}) > -\infty.$$

Assumption 2 $\nabla f(\mathbf{x})$ is L -Lipschitz smooth:

$$\forall \mathbf{x}, \mathbf{y} \in \mathbb{R}^d, \|\nabla f(\mathbf{x}) - \nabla f(\mathbf{y})\| \leq L \|\mathbf{x} - \mathbf{y}\|.$$

Assumption 3 The variance of the (mini-batch) stochastic gradients is bounded:

$$\mathbb{E} \left[\|\mathbf{g}(\mathbf{x}_t, \xi_t) - \nabla f(\mathbf{x}_t)\|^2 \right] \leq \sigma^2,$$

where $\sigma^2 > 0$ is a constant.

Assumption 4 Distributed workers might use stale models to compute gradients $\mathbf{g}(\mathbf{x}_{\tau_t}, \xi_t)$. We assume bounded staleness, that is: $t - S \leq \tau_t \leq t$. In other words, the model staleness τ_t satisfies the inequality $t - \tau_t \leq S$. We call $S \geq 0$ the maximum delay.

Assumption 5 Let the *expected cosine distance* be:

$$\frac{\mathbb{E} [\langle \Phi_k(\mathbf{g}(\mathbf{x}_{\tau_t}, \xi_t)), \nabla f(\mathbf{x}_t) \rangle]}{\mathbb{E} [\|\Phi_k(\mathbf{g}(\mathbf{x}_{\tau_t}, \xi_t))\| \|\nabla f(\mathbf{x}_t)\|]} = \mu_t \geq \mu.$$

We assume, similarly to previous work [11], that the constant $\mu > 0$ measures the discrepancy between the sparsified stochastic gradient and the full gradient.

Theorem 1. Let Assumptions 1–5 hold. Consider the memory-less sparsified SGD defined in Section 2, which uses the $\Phi_k(\cdot)$ top- k operator for a given $1 \leq k \leq d$. Then, for an appropriately defined learning rate $\eta_t = \frac{\rho\mu}{L\sqrt{t+1}}$ and for $\Lambda = \left(f(\mathbf{x}_0) - \inf_{\mathbf{x}} f(\mathbf{x})\right)$, it holds that:

$$\min_{0 \leq t \leq T} \mathbb{E} \left[\|\nabla f(\mathbf{x}_t)\|^2 \right] \leq \frac{\left(\sum_{t=0}^{T-1} \left(\frac{\eta_t^2 L}{2} \sigma^2 \right) \right) + \Lambda + C}{\sum_{t=0}^{T-1} \left(\eta_t \rho \mu - \frac{\eta_t^2 L}{2} \right)}.$$

Corollary 1. Let the conditions of Theorem 1 hold. Then for an appropriately defined constant learning rate $\eta_t = \eta = \frac{\rho\mu}{L\sqrt{T}}$, we have that:

$$\min_{0 \leq t \leq T} \mathbb{E} \left[\|\nabla f(\mathbf{x}_t)\|^2 \right] \leq \left(\frac{\sigma^2}{2} + \frac{(\Lambda + C)L}{(\rho\mu)^2} \right) \frac{1}{\sqrt{T} - \frac{1}{2}}.$$

Asymptotically, the convergence rate of memory-less sparsified SGD behaves as $\mathcal{O}(\frac{1}{\sqrt{T}})$, which matches the best known results for non-convex SGD [18], and for non-convex asynchronous SGD [24]. Note that considering a constant learning rate intuitively makes sense. When gradients are not heavily sparsified, i.e., ρ is large, we can afford a large learning rate. Similarly, when stale, sparse stochastic, and full gradients are similar, i.e., when μ is large, we can again set a large learning rate.

It is more difficult to quantify the role of the constant terms in Corollary 1, especially those involving sparsification. While it is evident that aggressive sparsification (extremely small ρ) could harm convergence, the exact role of the second constant term heavily depends on the initialization and the geometry of the loss function, which we do not address in this work. We thus resort to a numerical study to clarify these questions, but introduce a proxy for measuring convergence rate. Instead of imposing a target test accuracy, and use the number of training iterations to measure convergence rate (which we found to be extremely noisy), we fix an iteration budget, and measure the test accuracy once training concludes.

Remarks. A careful assessment of Assumption 5 is in order. We assume that a sparse version of a stochastic gradient computed with respect to a stale model, does not diverge too much from the true, full gradient¹. We measure this coherency through a positive constant $\mu > 0$. However, it is plausible to question the validity of such assumption, especially in a situation where either the sparsification is too aggressive, or the maximum delay is too high.

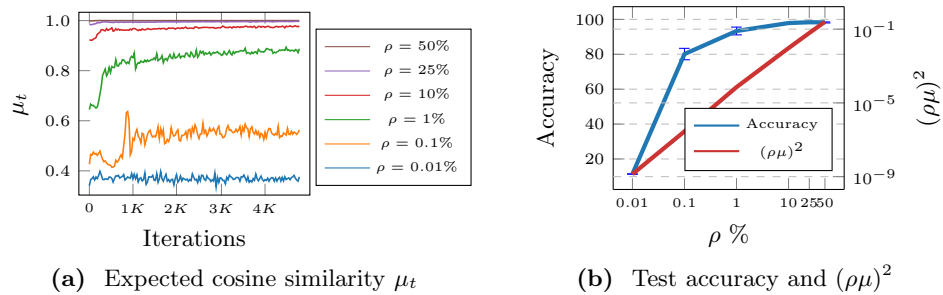


Fig. 1: Empirical results in support to Assumption 5. Experiments for ϕ SGD with LENET on MNIST, using a range of possible sparsification coefficients ρ .

We study the limits of our assumption empirically, and report our findings in Figure 1. The evolution of the expected cosine similarity μ_t defined in Assumption 5, reported here as a function of algorithmic progress, is in line with our assumption. Clearly, aggressive sparsification negatively impacts gradient coherency, as shown in Figure 1a. Moreover, as expected from Theorem 1, convergence rate measured through the proxy of test accuracy, also increases with $(\rho\mu)^2$. When sparsification is too aggressive, $(\rho\mu)^2$ is too small, which harms convergence.

¹ A similar remark, albeit without sparsification, has been made in [11].

3.1 Proof Sketch

We now give an outline of the proof of Theorem 1, whereas the full proof is available in Appendix A. Following standard practice in non-convex asynchronous settings [27,24], we settle for the weaker notion of ergodic convergence to a local minimum of the function f . Our strategy is to bound the expected sum-of-squares gradients of f . By the L -Lipshitz property of $\nabla f(x)$ (see Assumption 2), we have that:

$$\begin{aligned} f(\mathbf{x}_{t+1}) &\leq f(\mathbf{x}_t) + \langle \mathbf{x}_{t+1} - \mathbf{x}_t, \nabla f(\mathbf{x}_t) \rangle + \frac{L}{2} \|\mathbf{x}_{t+1} - \mathbf{x}_t\|^2 \\ &= f(\mathbf{x}_t) - \eta_t \langle \Phi_k[\mathbf{g}(\mathbf{x}_{\tau_t}, \xi_t)], \nabla f(\mathbf{x}_t) \rangle + \frac{\eta_t^2 L}{2} \|\Phi_k[\mathbf{g}(\mathbf{x}_{\tau_t}, \xi_t)]\|^2. \end{aligned} \quad (1)$$

The strategy to continue the proof is to find an upper bound for the term $\mathbb{E}[\|\Phi_k[\mathbf{g}(\mathbf{x}_{\tau_t}, \xi_t)]\|^2]$ and a lower bound for the term $\mathbb{E}[\langle \Phi_k[\mathbf{g}(\mathbf{x}_{\tau_t}, \xi_t)], \nabla f(\mathbf{x}_t) \rangle]$.

Let's focus on the term $\eta_t \langle \Phi_k[\mathbf{g}(\mathbf{x}_{\tau_t}, \xi_t)], \nabla f(\mathbf{x}_t) \rangle$. Using Lemma 1, Assumption 5, and some algebraic manipulations, we can bound the expectation of the above term as follows:

$$\mathbb{E}[\eta_t \langle \Phi_k[\mathbf{g}(\mathbf{x}_{\tau_t}, \xi_t)], \nabla f(\mathbf{x}_t) \rangle] \geq \eta_t \rho \mu \mathbb{E}[\|\nabla f(\mathbf{x}_t)\|^2],$$

where $\rho = k/d$, and μ is defined in Assumption 5.

Next, we can bound the expectation of the term $\frac{\eta_t^2 L}{2} \|\Phi_k[\mathbf{g}(\mathbf{x}_{\tau_t}, \xi_t)]\|^2$ by remarking that:

$$\mathbb{E}[\|\Phi_k[\mathbf{g}(\mathbf{x}_{\tau_t}, \xi_t)]\|^2] \leq \mathbb{E}[\|\nabla f(\mathbf{x}_{\tau_t})\|^2] + \sigma^2.$$

We then introduce a bound for the term:

$$\sum_{t=0}^{T-1} \eta_t^2 \mathbb{E}[\|\nabla f(\mathbf{x}_{\tau_t})\|^2] \leq \sum_{t=0}^{T-1} \eta_t^2 \mathbb{E}[\|\nabla f(\mathbf{x}_t)\|^2] + C,$$

where C is a positive finite constant.

Finally, if we take the expectation of the whole inequality 1, sum over t from 0 to $T-1$, use Assumption 1 and Assumption 5, the derivations above, and let $\Lambda = \left(f(\mathbf{x}_0) - \inf_{\mathbf{x}} f(\mathbf{x})\right)$, by rearranging we obtain:

$$\sum_{t=0}^{T-1} \left(\eta_t \rho \mu - \frac{L \eta_t^2}{2} \right) \mathbb{E}[\|\nabla f(\mathbf{x}_t)\|^2] \leq \Lambda + C + \frac{\sigma^2 L}{2} \sum_{t=0}^{T-1} \eta_t^2.$$

from which we derive the result of Theorem 1:

$$\min_{0 \leq t \leq T} \mathbb{E}[\|\nabla f(\mathbf{x}_t)\|^2] \leq \frac{\left(\sum_{t=0}^{T-1} \left(\frac{\eta_t^2 L}{2} \sigma^2 \right) \right) + \Lambda + C}{\sum_{t=0}^{T-1} \left(\eta_t \rho \mu - \frac{\eta_t^2 L}{2} \right)}.$$

Moreover, by choosing an appropriate constant learning rate ($\eta_t = \frac{\rho\mu}{L\sqrt{T}}$), we can derive Corollary 1:

$$\min_{0 \leq t \leq T} \mathbb{E} \left[\|\nabla f(\mathbf{x}_t)\|^2 \right] \leq \left(\frac{\sigma^2}{2} + \frac{(\Lambda + C)L}{(\rho\mu)^2} \right) \frac{1}{\sqrt{T} - \frac{1}{2}}.$$

4 Experiments

While the benefits of sparsification have been extensively validated in the literature [2,1,33,38,3], such works focus on communication costs in a synchronous setup, with the exception of the work in [35], which illustrates a simple experiment in a multi-core asynchronous setup. Instead, our experiments focus on verifying that: 1) the effects of staleness are negligible; 2) sparsification does not harm convergence rates, using test accuracy as a proxy; 3) the benefits of the memory mechanism applied to sparsified SGD. We consider several worker delay distributions, and we compare the performance of the three SGD variants: standard SGD, and sparsified SGD with and without memory. We also investigate the effects of scaling-out the system, by going up to 128 workers.

For our experimental campaign, we have built a custom simulator that plugs into existing machine learning libraries to leverage automatic differentiation and the vast availability of models, but abstracts away the complications of a real distributed setting. With this setup, it is easy to compare a variety of stochastic optimization algorithms on realistic and complex loss functions. More details about our simulator are given in Appendix B.

4.1 Experimental setup

SGD variants. We compare sparsified SGD without (ϕ SGD) and with memory (ϕ MEMSGD) to “vanilla” asynchronous SGD (ASGD). For all algorithms, and for all scenarios, we perform a grid search to find the best learning rate. When relevant, Figures report standard deviation, obtained by repeating our experiments 5 times. Note that for direct comparisons on individual experiments to be fair, we make sure to use the same algorithmic initialization for SGD (e.g., we use the same initial model parameters), and the same simulation seed.

Parameters. We configure the system architecture as follows: we consider a “parameter server” setup, whereby a given number of worker machines are connected to a master by a simple network model, we do not simulate network congestion, we impose fair bandwidth sharing, and we do not account for routing overheads.

In our simulations, both computation and communication costs can be modeled according to a variety of distributions. In this work we use uniformly distributed computation times with a small support, that are indicative of an homogeneous system. Instead of directly controlling the staleness of gradient updates, as done in other studies [12,11], we indirectly induce staleness by imposing synthetic network delays, which we generate according to an exponential distribution with rate λ (the inverse of the mean). In particular, each worker samples

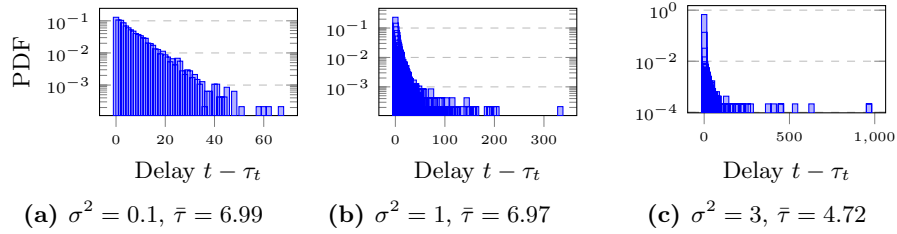


Fig. 2: Delay distributions of a simulation run with LENET on MNIST, in a distributed setting with 8 workers. For each worker we generate a network delay according to an exponential distribution with rate λ . We sample λ from a log-normal distribution with mean 0 and variance σ^2 . For each configuration, we also report the resulting average staleness $\bar{\tau}$.

a value for λ from a log-normal distribution with mean 0 and variance σ^2 . Figure 2 shows the resulting delay distribution for the entire training period in a simulation with 8 workers, using different values of σ^2 . As we increase σ^2 , the maximum delay experienced by the workers increases, up to very large values. In addition, the mass of the distribution shifts towards lower delays; indeed, for higher values of σ^2 , the majority of workers have small delays and only few workers experience very large delays. This is confirmed by the average staleness $\bar{\tau}$, which decreases as σ^2 increases. Notice that the interplay between communication delay and staleness is subtle: we provide a comprehensive description of the staleness generation process in Appendix B, with illustrations that help understanding the shape of the τ_t distribution.

Models and datasets. We consider a classification task, where we train two convolutional neural network (CNN) variants of increasing model complexity, to gain insight on the role of sparsification for large deep network models. First, we study the behavior of LENET, using the MNIST dataset, then we move on to RESNET-56, using the CIFAR10 dataset. The model parameter and gradients dimensionality are approximately $d \in \{60K, 600K\}$ for LENET and RESNET-56, respectively. We use a training mini-batch size of 64 for MNIST and 128 for RESNET-56 and a testing mini-batch size of 128 samples. Additional details are available in Appendix D.

4.2 Comparative analysis

We compare ϕ SGD and ϕ MEMSGD with ASGD by measuring the test accuracy reached after a fixed number of epochs, which we set to 5 for LENET on MNIST and 161 for RESNET-56 on CIFAR10. We consider three scenarios, with 8 workers: each has a different delay distribution, given by the parameter σ^2 , as shown in Figure 2. For sparsified methods, we use the best sparsification coefficient ρ . We discuss how ρ can be tuned in Section 4.3.

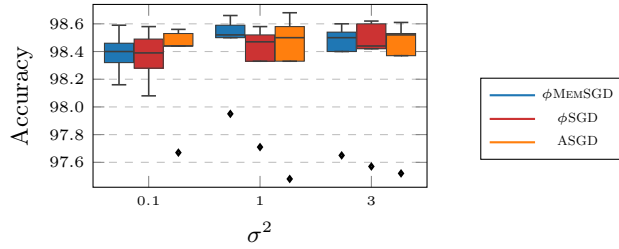


Fig. 3: Comparison of test accuracy of LENET on MNIST, for three different asynchronous settings with 8 workers. In each setting we sample the exponential rates λ from a log-normal distribution with mean 0 and variance σ^2 . For sparsified methods, the best ρ has been taken.

ϕMEMSGD	ϕSGD	ASGD
87.05 ± 0.53	86.21 ± 1.06	85.90 ± 1.01

Table 1: Comparison of test accuracy of RESNET-56 on CIFAR10, with $\sigma^2 = 0.1$.

Figure 3 illustrates results obtained using a LENET architecture with the MNIST dataset, while Table 1 reports the results obtained with RESNET-56 on CIFAR10, fixing $\sigma^2 = 0.1$.

Clearly, for both simple and deep models, the effects of sparsification on test accuracy are negligible. Given a reasonable choice of sparsification ρ , all variants achieve similar test accuracy using the same number of training iterations. Moreover, sparsified methods consistently achieve comparable performance to the non-sparse method irrespectively of the delay distribution. This confirms the result in Corollary 1, which indicates asymptotically vanishing effects of staleness on convergence (indeed, the term τ does not appear in the bound). We also observe that, as expected, the memory-based variant of sparsified SGD has an edge on the memory-less method, because it achieves better performance for lower values of ρ . This results clarifies the impact of memory-based error correction as a method to recover lost information due to aggressive sparsification.

Finally, note that we explicitly do not compare the methods using wall-clock times, as we are not interested in measuring the well-known benefits of sparsification in terms of reduced communication costs.

4.3 Tuning gradient sparsification

Using theorem 1 alone, it can be difficult to understand how ρ can be tuned. Next, we focus on the LENET architecture using the MNIST, trained for 5 epochs, to understand how this affects the accuracy of sparsified SGD.

The results in Figure 4 show the impact of different values of the sparsification coefficient ρ on test accuracy. We notice a stark difference between ϕMEMSGD and ϕSGD : the latter is much more sensitive to appropriate choices of ρ , and

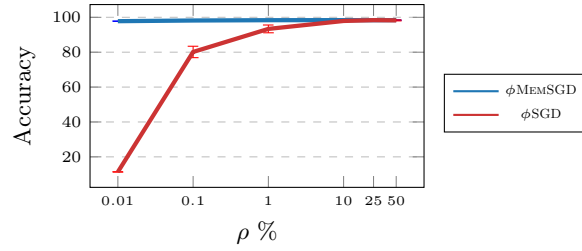


Fig. 4: Detailed study to understand how to tune the sparsification ρ , for LENET on MNIST. Test accuracy as a function of ρ , in a system with 8 workers and $\sigma^2 = 0.1$

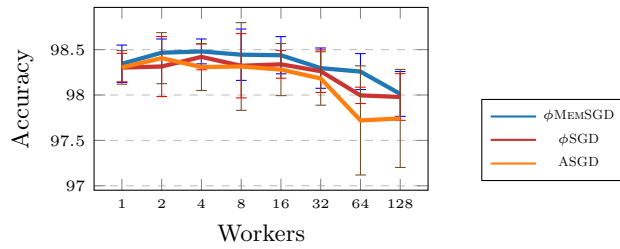


Fig. 5: Comparison of test accuracy, as a function of the number of workers. Results for LENET on MNIST.

requires larger coefficients to achieve a reasonable test accuracy. For ϕ MEMSGD, instead, aggressive sparsification doesn't penalize performance noticeably, thanks to the memory mechanism. Then, even aggressive sparsification can be viable, as the cost per iteration (in terms of transmission times) decreases drastically, compared to standard SGD. Also, note that the top- k operator can be executed efficiently on GPUs [34], so that computational costs per iteration are equivalent to standard SGD.

4.4 Scalability

We now investigate how the three SGD variants scale with an increasing number of workers. As shown in Figure 5, all variants of SGD incur a slight drop in performance with more workers. Indeed, with more workers, the delay distribution in the system changes according to Figure 2, due to an increase in the probability of picking large delays. We note again that applying sparsification does not harm the performance of SGD, in that both ϕ MEMSGD and ϕ SGD reach a comparable test accuracy with respect to ASGD. This is valid also for a deep convolutional network: for example, we run RESNET-56 on CIFAR10 with 32 workers and we obtained a test accuracy of 85.30 ± 1.24 for ASGD and 86.01 ± 0.49 for ϕ MEMSGD with a sparsification coefficient $\rho = 1\%$.

Our results reinforce the message that sparsified SGD should be preferred over vanilla SGD, and this carries over to large scale scenarios in which, other-

wise, excessively large message sizes could entail network congestion and jeopardize algorithmic efficiency.

5 Conclusion

In this work we focused on the role of sparsification methods applied to distributed stochastic optimization of non-convex loss functions, typically found in many modern machine learning settings.

For the first time, we provided a simple and concise analysis of the joint effects of asynchronicity and sparsification on mini-batch SGD, and showed that it converges asymptotically as $\mathcal{O}\left(1/\sqrt{T}\right)$. Intuitively, top- k sparsification restricts the path taken by model iterates in the optimization landscape to follow the principal components of a stochastic gradient update, as also noticed in [4].

We complemented our theoretical results with a thorough empirical campaign. Our experiments covered both variants of sparsified SGD, with and without memory, and compared them to standard SGD. We used a simple system simulator, which allowed us to explore scenarios with different delay distributions, as well as an increasing number of workers.

Our results substantiated the theoretical findings of this work: the effects of staleness vanish asymptotically, and the impact of sparsification is negligible on convergence rate and test accuracy. We also studied how to appropriately choose the sparsification factor, and concluded that the memory mechanism applied to sparsified SGD allows to substantially sparsify gradients, save on communication costs, while obtaining comparable performance to standard SGD.

Our future plan is to establish a connection between gradient sparsification and recent studies showing that the landscape of the loss surface of deep models is typically sparse [32,15,22]. In light of such works, [17] suggests that sparsification can be directly applied to model parameters, albeit training requires multiple stages. Gradient sparsification could then be studied as a mechanism to favor model compression at training time.

References

1. Dryden, N., Moon, T., Jacobs, S.A., Essen, B.V.: Communication quantization for data-parallel training of deep neural networks. In: 2016 2nd Workshop on Machine Learning in HPC Environments (MLHPC). pp. 1–8 (Nov 2016). <https://doi.org/10.1109/MLHPC.2016.004>
2. Aji, A.F., Heafield, K.: Sparse communication for distributed gradient descent. arXiv **abs/1704.05021** (2017), <http://arxiv.org/abs/1704.05021>
3. Alistarh, D., Grubic, D., Li, J., Tomioka, R., Vojnovic, M.: QSGD : Communication-efficient SGD via gradient quantization and encoding. In: Advances in Neural Information Processing Systems 30, pp. 1709–1720. Curran Associates, Inc. (2017), <http://papers.nips.cc/paper/6768-qsgd-communication-efficient-sgd-via-gradient-quantization-and-en>

4. Alistarh, D., Hoeffler, T., Johansson, M., Konstantinov, N., Khirirat, S., Renggli, C.: The convergence of sparsified gradient methods. In: Bengio, S., Wallach, H., Larochelle, H., Grauman, K., Cesa-Bianchi, N., Garnett, R. (eds.) *Advances in Neural Information Processing Systems*, pp. 5973–5983. Curran Associates, Inc. (2018), <http://papers.nips.cc/paper/7837-the-convergence-of-sparsified-gradient-methods.pdf>
5. Bernstein, J., Wang, Y.X., Azizzadenesheli, K., Anandkumar, A.: Compression by the signs: distributed learning is a two-way street. In: *ICLR* (2018)
6. Bernstein, J., Wang, Y.X., Azizzadenesheli, K., Anandkumar, A.: signsgd: Compressed optimisation for non-convex problems. *Proceedings of Machine Learning Research* **80**, 560–569 (2018)
7. Bottou, L.: Large-scale machine learning with stochastic gradient descent. In: *Proceedings of COMPSTAT'2010*, pp. 177–186. Springer (2010)
8. Bottou, L., Curtis, F.E., Nocedal, J.: Optimization methods for large-scale machine learning. *SIAM Review* **60**(2), 223–311 (2018). <https://doi.org/10.1137/16M1080173>, <https://doi.org/10.1137/16M1080173>
9. Chen, J., Monga, R., Bengio, S., Jozefowicz, R.: Revisiting distributed synchronous sgd. In: *International Conference on Learning Representations Workshop Track* (2016), <https://arxiv.org/abs/1604.00981>
10. Chilimbi, T., Suzue, Y., Apacible, J., Kalyanaraman, K.: Project adam: Building an efficient and scalable deep learning training system. In: *11th USENIX Symposium on Operating Systems Design and Implementation (OSDI 14)*. pp. 571–582. USENIX Association, Broomfield, CO (2014), <https://www.usenix.org/conference/osdi14/technical-sessions/presentation/chilimbi>
11. Dai, W., Zhou, Y., Dong, N., Zhang, H., Xing, E.P.: Toward understanding the impact of staleness in distributed machine learning. In: *Proceedings of the 7th International Conference on Learning Representations. ICLR'19* (2019)
12. Damaskinos, G., El Mhamdi, E.M., Guerraoui, R., Patra, R., Taziki, M.: Asynchronous byzantine machine learning (the case of sgd). In: Dy, J., Krause, A. (eds.) *Proceedings of the 35th International Conference on Machine Learning. Proceedings of Machine Learning Research*, vol. 80, pp. 1145–1154. PMLR, Stockholm, Sweden (10–15 Jul 2018), <http://proceedings.mlr.press/v80/damaskinos18a.html>
13. De Sa, C.M., Zhang, C., Olukotun, K., Re, C.: Taming the wild: A unified analysis of hogwild-style algorithms. In: *Advances in neural information processing systems*. pp. 2674–2682 (2015)
14. Dean, J., Corrado, G., Monga, R., Chen, K., Devin, M., Mao, M., aurelio Ranzato, M., Senior, A., Tucker, P., Yang, K., Le, Q.V., Ng, A.Y.: Large scale distributed deep networks. In: Pereira, F., Burges, C.J.C., Bottou, L., Weinberger, K.Q. (eds.) *Advances in Neural Information Processing Systems 25*, pp. 1223–1231. Curran Associates, Inc. (2012), <http://papers.nips.cc/paper/4687-large-scale-distributed-deep-networks.pdf>
15. Draxler, F., Veschgini, K., Salmhofer, M., Hamprecht, F.A.: Essentially no barriers in neural network energy landscape. *arXiv preprint arXiv:1803.00885* (2018)
16. Dutta, S., Joshi, G., Ghosh, S., Dube, P., Nagpurkar, P.: Slow and stale gradients can win the race: Error-runtime trade-offs in distributed SGD . In: Storkey, A., Perez-Cruz, F. (eds.) *Proceedings of the Twenty-First International Conference on Artificial Intelligence and Statistics*. pp. 803–812. PMLR (2018), <http://proceedings.mlr.press/v84/dutta18a.html>
17. Frankle, J., Carbin, M.: The lottery ticket hypothesis: Finding sparse, trainable neural networks. In: *ICLR* (2019)

18. Ghadimi, S., Lan, G.: Stochastic first-and zeroth-order methods for nonconvex stochastic programming. *SIAM Journal on Optimization* **23**(4), 2341–2368 (2013)
19. Goyal, P., Dollar, P., Girshick, R.B., Noordhuis, P., Wesolowski, L., Kyrola, A., Tulloch, A., Jia, Y., He, K.: Accurate, large minibatch sgd: Training i mage net in 1 hour. *arXiv abs/1706.02677* (2017)
20. Ho, Q., Cipar, J., Cui, H., Lee, S., Kim, J.K., Gibbons, P.B., Gibson, G.A., Ganger, G., Xing, E.P.: More effective distributed ML via a stale synchronous parallel parameter server. In: Burges, C.J.C., Bottou, L., Welling, M., Ghahramani, Z., Weinberger, K.Q. (eds.) *Advances in Neural Information Processing Systems 26*, pp. 1223–1231. Curran Associates, Inc. (2013), <http://papers.nips.cc/paper/4894-more-effective-distributed-ml-via-a-stale-synchronous-parallel-parameter-server>
21. Jiang, J., Cui, B., Zhang, C., Yu, L.: Heterogeneity-aware distributed parameter servers. In: *Proceedings of the 2017 ACM International Conference on Management of Data*. pp. 463–478. SIGMOD ’17, ACM, New York, NY, USA (2017). <https://doi.org/10.1145/3035918.3035933>, <http://doi.acm.org/10.1145/3035918.3035933>
22. Karakida, R., Akaho, S., Amari, S.i.: Universal statistics of fisher information in deep neural networks: mean field approach. *arXiv preprint arXiv:1806.01316* (2018)
23. Li, M., Andersen, D.G., Park, J.W., Smola, A.J., Ahmed, A., Josifovski, V., Long, J., Shekita, E.J., Su, B.Y.: Scaling distributed machine learning with the parameter server. In: *11th USENIX Symposium on Operating Systems Design and Implementation (OSDI 14)*. pp. 583–598. USENIX Association, Broomfield, CO (2014), <https://www.usenix.org/conference/osdi14/technical-sessions/presentation/li-mu>
24. Lian, X., Huang, Y., Li, Y., Liu, J.: Asynchronous parallel stochastic gradient for nonconvex optimization. In: *Advances in Neural Information Processing Systems*. pp. 2737–2745 (2015)
25. Lin, T., Stich, S.U., Jaggi, M.: Don’t use large mini-batches, use local SGD. *arXiv, abs/1808.07217* (2018)
26. Lin, Y., Han, S., Mao, H., Wang, Y., Dally, B.: Deep gradient compression: Reducing the communication bandwidth for distributed training. In: *International Conference on Learning Representations* (2018), <https://openreview.net/forum?id=SkhQHMWOW>
27. Liu, J., Wright, S.J.: Asynchronous stochastic coordinate descent: Parallelism and convergence properties. *SIAM Journal on Optimization* **25**(1), 351–376 (2015)
28. Mitliagkas, I., Zhang, C., Hadjis, S., Re, C.: Asynchrony begets momentum, with an application to deep learning. In: *2016 54th Annual Allerton Conference on Communication, Control, and Computing (Allerton)*. pp. 997–1004. IEEE (2016)
29. Moulines, E., Bach, F.R.: Non-asymptotic analysis of stochastic approximation algorithms for machine learning. In: Shawe-Taylor, J., Zemel, R.S., Bartlett, P.L., Pereira, F., Weinberger, K.Q. (eds.) *Advances in Neural Information Processing Systems 24*, pp. 451–459. Curran Associates, Inc. (2011), <http://papers.nips.cc/paper/4316-non-asymptotic-analysis-of-stochastic-approximation-algorithms-for-machine-learning>
30. Recht, B., Re, C., Wright, S., Niu, F.: Hogwild: A lock-free approach to parallelizing stochastic gradient descent. In: Shawe-Taylor, J., Zemel, R.S., Bartlett, P.L., Pereira, F., Weinberger, K.Q. (eds.) *Advances in Neural Information Processing Systems*, pp. 693–701. Curran Associates, Inc. (2011), <http://papers.nips.cc/paper/4390-hogwild-a-lock-free-approach-to-parallelizing-stochastic-gradient-descent>
31. Robbins, H., Monro, S.: A stochastic approximation method. *Annals of Mathematical Statistics* **22**, 400–407 (1951)

32. Sagun, L., Evci, U., Guney, V.U., Dauphin, Y., Bottou, L.: Empirical analysis of the hessian of over-parametrized neural networks. arXiv preprint arXiv:1706.04454 (2017)
33. Seide, F., Fu, H., Droppo, J., Li, G., Yu, D.: 1-bit stochastic gradient descent and its application to data-parallel distributed training of speech DNN s. In: Fifteenth Annual Conference of the International Speech Communication Association (2014)
34. Shanbhag, A., Pirk, H., Madden, S.: Efficient top-k query processing on massively parallel hardware. In: Proceedings of the 2018 International Conference on Management of Data. pp. 1557–1570. ACM (2018)
35. Stich, S.U., Cordonnier, J.B., Jaggi, M.: Sparsified SGD with memory. In: Bengio, S., Wallach, H., Larochelle, H., Grauman, K., Cesa-Bianchi, N., Garnett, R. (eds.) Advances in Neural Information Processing Systems 31, pp. 4447–4458. Curran Associates, Inc. (2018), <http://papers.nips.cc/paper/7697-sparsified-sgd-with-memory.pdf>
36. Stich, S.U., Karimireddy, S.P.: The error-feedback framework: Better rates for sgd with delayed gradients and compressed communication (2019)
37. Stich, S.U.: Local SGD converges fast and communicates little. In: Proceedings of the 7th International Conference on Learning Representations. ICLR’19 (2019)
38. Strom, N.: Scalable distributed DNN training using commodity GPU cloud computing. In: Sixteenth Annual Conference of the International Speech Communication Association (2015)
39. Wangni, J., Wang, J., Liu, J., Zhang, T.: Gradient sparsification for communication-efficient distributed optimization. In: Bengio, S., Wallach, H., Larochelle, H., Grauman, K., Cesa-Bianchi, N., Garnett, R. (eds.) Advances in Neural Information Processing Systems, pp. 1299–1309. Curran Associates, Inc. (2018), <http://papers.nips.cc/paper/7405-gradient-sparsification-for-communication-efficient-distributed-optimization.pdf>
40. Wen, W., Xu, C., Yan, F., Wu, C., Wang, Y., Chen, Y., Li, H.: Terngrad: Ternary gradients to reduce communication in distributed deep learning. In: Guyon, I., Luxburg, U.V., Bengio, S., Wallach, H., Fergus, R., Vishwanathan, S., Garnett, R. (eds.) Advances in Neural Information Processing Systems 30, pp. 1509–1519. Curran Associates, Inc. (2017), <http://papers.nips.cc/paper/6749-terngrad-ternary-gradients-to-reduce-communication-in-distributed-deep-learning.pdf>
41. You, Y., Gitman, I., Ginsburg, B.: Scaling sgd batch size to 32k for image net training. arXiv, abs/1708.03888 **6** (2017)
42. Yu, H., Yang, S., Zhu, S.: Parallel restarted SGD with faster convergence and less communication: Demystifying why model averaging works for deep learning. In: AAAI 2019 (2019)
43. Zhang, J., Sa, C.D., Mitliagkas, I., Re, C.: Parallel sgd: When does averaging help? arXiv abs/1606.07365 (2016)

A Proof of Theorem

In this section we build all the useful tools to formalize the proof of Theorem 1. In Appendix A.1 we prove the k -contraction lemma, in Appendix A.2 we restate assumptions for simplicity, we derive useful facts in Appendix A.3, derive a tighter bounding term for the sum of magnitudes of stale gradients in Appendix A.4, and finally derive the full proof of the convergence theorem in Appendix A.5.

A.1 Proof of Lemma 1

Given a vector $\mathbf{u} \in \mathbb{R}^d$, a parameter $1 \leq k \leq d$, and the top- k operator $\Phi_k(\mathbf{u}) : \mathbb{R}^d \rightarrow \mathbb{R}^d$ defined in Definition 1, we have that:

$$\|\Phi_k(\mathbf{u})\|^2 \geq \frac{k}{d} \|\mathbf{u}\|^2$$

In fact we can write $\|\mathbf{u}\|^2$ as follows:

$$\begin{aligned} \|\Phi_k(\mathbf{u})\|^2 &= \|\mathbf{u}\|^2 - \|\mathbf{u} - \Phi_k \mathbf{u}\|^2 \\ &\geq \|\mathbf{u}\|^2 - \left(1 - \frac{k}{d}\right) \|\mathbf{u}\|^2 \\ &\geq \frac{k}{d} \|\mathbf{u}\|^2 \end{aligned} \tag{2}$$

Where the inequality is obtained by simply applying the k -contraction property.

A.2 Recap of Assumptions

We start by rewriting for simplicity Assumption 1 to Assumption 5:

1. $f(\mathbf{x})$ is continuously differentiable and bounded below: $\inf_x f(\mathbf{x}) > -\infty$
2. $\nabla f(\mathbf{x})$ is L -Lipschitz smooth:

$$\forall \mathbf{x}, \mathbf{y} \in \mathbb{R}^d, \|\nabla f(\mathbf{x}) - \nabla f(\mathbf{y})\| \leq L \|\mathbf{x} - \mathbf{y}\|$$

3. The variance of the (mini-batch) stochastic gradients is bounded:

$$\mathbb{E} \left[\|\mathbf{g}(\mathbf{x}_t, \xi_t) - \nabla f(\mathbf{x}_t)\|^2 \right] \leq \sigma^2,$$

where $\sigma^2 > 0$ is a constant.

4. The staleness is bounded, that is: $t - S \leq \tau_t \leq t$, $S \geq 0$. In other words, the model staleness τ_t satisfies the inequality $t - \tau_t \leq S$. We call $S \geq 0$ the maximum delay.
5. The cosine distance between sparse, stale and stochastic gradient and the full one is lower bounded

$$\frac{\mathbb{E} [\langle \Phi_k(\mathbf{g}(\mathbf{x}_{\tau_t}, \xi_t)), \nabla f(\mathbf{x}_t) \rangle]}{\mathbb{E} [\|\Phi_k(\mathbf{g}(\mathbf{x}_{\tau_t}, \xi_t))\| \|\nabla f(\mathbf{x}_t)\|]} = \mu_t \geq \mu$$

Notice moreover that ξ_t is statistically independent from $\{\mathbf{x}_0, \dots, \mathbf{x}_t\}$.

A.3 Useful facts

Starting from Assumption 2 we can write that:

$$f(\mathbf{x}) \leq f(\mathbf{y}) + \langle \mathbf{x} - \mathbf{y}, \nabla f(\mathbf{y}) \rangle + \frac{L}{2} \|\mathbf{x} - \mathbf{y}\|^2 \quad \forall \mathbf{x}, \mathbf{y}$$

Trivially we can rewrite this inequality by using as arguments the two vectors $\mathbf{x}_t, \mathbf{x}_{t+1}$:

$$\begin{aligned}
f(\mathbf{x}_{t+1}) &\leq f(\mathbf{x}_t) + \langle \mathbf{x}_{t+1} - \mathbf{x}_t, \nabla f(\mathbf{x}_t) \rangle + \\
&\quad + \frac{L}{2} \|\mathbf{x}_{t+1} - \mathbf{x}_t\|^2 \\
&= f(\mathbf{x}_t) - \eta_t \langle \Phi_k[\mathbf{g}(\mathbf{x}_{\tau_t}, \xi_t)], \nabla f(\mathbf{x}_t) \rangle \\
&\quad + \frac{\eta_t^2 L}{2} \|\Phi_k[\mathbf{g}(\mathbf{x}_{\tau_t}, \xi_t)]\|^2
\end{aligned} \tag{3}$$

where the last equality is due to $\mathbf{x}_{t+1} = \mathbf{x}_t - \eta_t \Phi_k(\mathbf{g}(\mathbf{x}_{\tau_t}, \xi_t))$. Notice that even if \mathbf{x}_t as well as ξ_t, τ_t and consequently $f(\mathbf{x}_t)$ and $g(\mathbf{x}_t)$ are random processes, due to the geometric constraints imposed on the cost function, the above inequality holds with probability 1.

The second useful quantity we derive is a bound for squared magnitude of $\mathbf{g}(\mathbf{x}_t, \xi_t)$. We start with Assumption 3.

Before proceeding, we introduce the following notation: Ω is the set of ALL random variables (i.e. $\Omega = \{\xi_0, \dots, \xi_t, \mathbf{x}_0, \dots, \mathbf{x}_t, \tau_0, \dots, \tau_t\}$), furthermore, we indicate with $\sim \xi_t$ the set difference between Ω and ξ_t .

We write:

$$\begin{aligned}
&\mathbb{E}_\Omega [\|\mathbf{g}(\mathbf{x}_t, \xi_t) - \nabla f(\mathbf{x}_t)\|^2] \\
&= \mathbb{E}_\Omega [\|\mathbf{g}(\mathbf{x}_t, \xi_t) - \mathbb{E}_{\xi_t}(\mathbf{g}(\mathbf{x}_t, \xi_t))\|^2] \\
&= \mathbb{E}_{\sim \xi_t} [\mathbb{E}_{\xi_t} [\|\mathbf{g}(\mathbf{x}_t, \xi_t) - \mathbb{E}_{\xi_t}(\mathbf{g}(\mathbf{x}_t, \xi_t))\|^2]] \\
&= \mathbb{E}_{\sim \xi_t} [\mathbb{E}_{\xi_t} [\|\mathbf{g}(\mathbf{x}_t, \xi_t)\|^2] - \|\mathbb{E}_{\xi_t}(\mathbf{g}(\mathbf{x}_t, \xi_t))\|^2] \\
&= \mathbb{E}_\Omega [\|\mathbf{g}(\mathbf{x}_t, \xi_t)\|^2] - \mathbb{E}_\Omega [\|\nabla f(\mathbf{x}_t)\|^2] \leq \sigma^2
\end{aligned}$$

from which:

$$\mathbb{E}_\Omega [\|\mathbf{g}(\mathbf{x}_t, \xi_t)\|^2] \leq \mathbb{E}_\Omega [\|\nabla f(\mathbf{x}_t)\|^2] + \sigma^2 \tag{4}$$

A.4 Bounding magnitudes of delayed gradients

Differently from [11], we derive a tighter bound for the following term:

$$\sum_{t=0}^{T-1} \eta_t^2 \mathbb{E} [\|\nabla f(\mathbf{x}_{\tau_t})\|^2] \tag{5}$$

Indeed, thanks to the fact that η_t is a decreasing sequence, and using the law of total expectation:

$$\begin{aligned}
& \sum_{t=0}^{T-1} \eta_t^2 \mathbb{E} \left[\|\nabla f(\mathbf{x}_{\tau_t})\|^2 \right] \\
&= \sum_{t=0}^{T-1} \eta_t^2 \sum_{l=t-S}^t \Pr(\tau_t = l) \mathbb{E} \left[\|\nabla f(\mathbf{x}_l)\|^2 \right] \\
&\leq \sum_{t=0}^{T-1} \sum_{l=t-S}^t \eta_t^2 \Pr(\tau_t = l) \mathbb{E} \left[\|\nabla f(\mathbf{x}_l)\|^2 \right]
\end{aligned}$$

Before proceeding, it is useful to introduce a new random quantity, the delay D , distributed according to some probability density function $\Pr(D = i) = \pi_i$. Notice that the true relationship between $\Pr(\tau_t)$ and $\Pr(D)$ is:

$$\Pr(\tau_t = l) = \frac{\pi_{t-l}}{\sum_{i=0}^{\min(t,S)} \pi_i}.$$

Since $t - S \leq \tau_t \leq t$, obviously the delay variable D has support boundend in $[0, S]$. Moreover, to reduce clutter, we define: $\psi_l = \eta_l^2 \mathbb{E} \left[\|\nabla f(\mathbf{x}_l)\|^2 \right]$.

Now, we can continue our derivation as:

$$\begin{aligned}
& \sum_{t=0}^{T-1} \sum_{l=t-S}^t \frac{\pi_{t-l}}{\sum_{i=0}^{\min(t,S)} \pi_i} \psi_l = \\
& \frac{\pi_S \psi_{-S+0} + \pi_{S-1} \psi_{-S+1} + \cdots + \pi_1 \psi_{-1} + \pi_0 \psi_0}{\pi_0} + \\
& \frac{\pi_S \psi_{-S+1} + \pi_{S-1} \psi_{-S+2} + \cdots + \pi_1 \psi_0 + \pi_0 \psi_1}{\pi_0 + \pi_1} + \\
& \frac{\pi_S \psi_{-S+2} + \pi_{S-1} \psi_{-S+3} + \cdots + \pi_1 \psi_1 + \pi_0 \psi_2}{\pi_0 + \pi_1 + \pi_2} + \\
& \frac{\pi_S \psi_{-S+3} + \pi_{S-1} \psi_{-S+4} + \cdots + \pi_1 \psi_2 + \pi_0 \psi_3}{\pi_0 + \pi_1 + \pi_2 + \pi_3} + \\
& \dots \\
& \frac{\pi_S \psi_{T-S} + \dots + \pi_1 \psi_{T-1} + \pi_0 \psi_T}{1} \leq \\
& \pi_S \psi_{-S+0} + \pi_{S-1} \psi_{-S+1} + \cdots + \pi_1 \psi_{-1} + \pi_0 \psi_0 + C_0 + \\
& \pi_S \psi_{-S+1} + \pi_{S-1} \psi_{-S+2} + \cdots + \pi_1 \psi_0 + \pi_0 \psi_1 + C_1 + \\
& \pi_S \psi_{-S+2} + \pi_{S-1} \psi_{-S+3} + \cdots + \pi_1 \psi_1 + \pi_0 \psi_2 + C_2 + \\
& \pi_S \psi_{-S+3} + \pi_{S-1} \psi_{-S+4} + \cdots + \pi_1 \psi_2 + \pi_0 \psi_3 + C_3 + \\
& \dots \\
& \pi_S \psi_{T-S} + \dots + \pi_1 \psi_{T-1} + \pi_0 \psi_T + 0 \\
& \leq \sum_{t=0}^{T-1} \psi_t + C \\
& = \sum_{t=0}^{T-1} \eta_t^2 \mathbb{E} \left[\|\nabla f(\mathbf{x}_t)\|^2 \right] + C
\end{aligned}$$

where C is a suitable, finite, constant. We thus proved a strict bound on the sum of magnitudes of delayed gradients as

$$\sum_{t=0}^{T-1} \eta_t^2 \mathbb{E} \left[\|\nabla f(\mathbf{x}_{\tau_t})\|^2 \right] \leq \sum_{t=0}^{T-1} \eta_t^2 \mathbb{E} \left[\|\nabla f(\mathbf{x}_t)\|^2 \right] + C.$$

A.5 Derivation of the theorem

We start the derivation from Equation (3). We rearrange the inequality to bound the increment of cost function at time instant t as:

$$\begin{aligned}
f(\mathbf{x}_{t+1}) - f(\mathbf{x}_t) & \leq -\eta_t \langle \Phi_k[\mathbf{g}(\mathbf{x}_{\tau_t}, \xi_t)], \nabla f(\mathbf{x}_t) \rangle \\
& \quad + \frac{\eta_t^2 L}{2} \|\Phi_k[\mathbf{g}(\mathbf{x}_{\tau_t}, \xi_t)]\|^2
\end{aligned}$$

Written in this form, we are still dealing with random quantities. We are interested in taking the expectation of above inequality with respect to **all** random processes. Then:

$$\begin{aligned} & \mathbb{E}_\Omega [f(\mathbf{x}_{t+1}) - f(\mathbf{x}_t)] \\ & \leq \mathbb{E}_\Omega \left[-\eta_t \langle \Phi_k[\mathbf{g}(\mathbf{x}_{\tau_t}, \xi_t)], \nabla f(\mathbf{x}_t) \rangle + \frac{\eta_t^2 L}{2} \|\Phi_k[\mathbf{g}(\mathbf{x}_{\tau_t}, \xi_t)]\|^2 \right] \end{aligned}$$

The strategy to continue the proof is to find an upper bound for the expectation term $\mathbb{E}_\Omega [\|\Phi_k[\mathbf{g}(\mathbf{x}_{\tau_t}, \xi_t)]\|^2]$ and a lower bound for the expectation term $\mathbb{E}_\Omega [\langle \Phi_k[\mathbf{g}(\mathbf{x}_{\tau_t}, \xi_t)], \nabla f(\mathbf{x}_t) \rangle]$. We start with the upper bound as:

$$\begin{aligned} \mathbb{E}_\Omega [\|\Phi_k[\mathbf{g}(\mathbf{x}_{\tau_t}, \xi_t)]\|^2] & \leq \mathbb{E}_\Omega [\|\mathbf{g}(\mathbf{x}_{\tau_t}, \xi_t)\|^2] \\ & \leq \mathbb{E} [\|\nabla f(\mathbf{x}_{\tau_t})\|^2] + \sigma^2, \end{aligned}$$

where the first inequality is a trivial consequence of sparsification and the second is the application of Equation (4).

As anticipated, we aim at lower bounding the term: $\mathbb{E}_\Omega [\langle \Phi_k[\mathbf{g}(\mathbf{x}_{\tau_t}, \xi_t)], \nabla f(\mathbf{x}_t) \rangle]$. We start with Assumption 5 and write:

$$\begin{aligned} & \mathbb{E}_\Omega [\langle \Phi_k(\mathbf{g}(\mathbf{x}_{\tau_t}, \xi_t)), \nabla f(\mathbf{x}_t) \rangle] \\ & \geq \mu \mathbb{E}_\Omega [\|\Phi_k(\mathbf{g}(\mathbf{x}_{\tau_t}, \xi_t))\| \|\nabla f(\mathbf{x}_t)\|] \\ & = \mu \mathbb{E}_{\sim \xi_t} [\mathbb{E}_{\xi_t} [\|\Phi_k(\mathbf{g}(\mathbf{x}_{\tau_t}, \xi_t))\| \|\nabla f(\mathbf{x}_t)\|]] \\ & = \mu \mathbb{E}_{\sim \xi_t} [\mathbb{E}_{\xi_t} [\|\Phi_k(\mathbf{g}(\mathbf{x}_{\tau_t}, \xi_t))\|] \|\nabla f(\mathbf{x}_t)\|] \end{aligned}$$

We focus on the term $\mathbb{E}_{\xi_t} [\|\Phi_k(\mathbf{g}(\mathbf{x}_{\tau_t}, \xi_t))\|]$ and, thanks to the k -contraction property and the inequality of the norm of expected values, we can write:

$$\begin{aligned} & \mathbb{E}_\Omega [\langle \Phi_k(\mathbf{g}(\mathbf{x}_{\tau_t}, \xi_t)), \nabla f(\mathbf{x}_t) \rangle] \\ & \geq \mu \rho \mathbb{E}_{\sim \xi_t} [\mathbb{E}_{\xi_t} [\|\mathbf{g}(\mathbf{x}_{\tau_t}, \xi_t)\|] \|\nabla f(\mathbf{x}_t)\|] \\ & \geq \mu \rho \mathbb{E}_{\sim \xi_t} [\|\mathbb{E}_{\xi_t} [\mathbf{g}(\mathbf{x}_{\tau_t}, \xi_t)]\| \|\nabla f(\mathbf{x}_t)\|] \\ & = \mu \rho \mathbb{E}_{\sim \xi_t} [\|\nabla f(\mathbf{x}_{\tau_t})\| \|\nabla f(\mathbf{x}_t)\|] \end{aligned}$$

Before proceeding, we reasonably assume that:

$$\mathbb{E}_{\sim \xi_t} [\|\nabla f(\mathbf{x}_{\tau_t})\| \|\nabla f(\mathbf{x}_t)\|] \geq \mathbb{E}_{\sim \xi_t} [\|\nabla f(\mathbf{x}_t)\|^2], \quad (6)$$

since stale versions of the gradient should be larger, in magnitude, than recent versions.

Combining everything together we rewrite our initial inequality as:

$$\begin{aligned} \Delta_t = \mathbb{E}_\Omega [f(\mathbf{x}_{t+1}) - f(\mathbf{x}_t)] & \leq -\eta_t \rho \mu \mathbb{E}_{\sim \xi_t} [\|\nabla f(\mathbf{x}_t)\|^2] \\ & + \frac{\eta_t^2 L}{2} \left(\mathbb{E}_{\sim \xi_t} [\|\nabla f(\mathbf{x}_{\tau_t})\|^2] + \sigma^2 \right). \end{aligned}$$

To derive a convergence bound it is necessary to sum all the increments over t from 0 to T :

$$\begin{aligned}
\sum_{t=0}^{T-1} \Delta_t &\leq \sum_{t=0}^{T-1} \left(-\eta_t \rho \mu \mathbb{E}_{\sim \xi_t} [\|\nabla f(\mathbf{x}_t)\|^2] + \right. \\
&\quad \left. \frac{\eta_t^2 L}{2} \left(\mathbb{E}_{\sim \xi_t} [\|\nabla f(\mathbf{x}_t)\|^2] + \sigma^2 \right) \right) \\
&\leq \left(\sum_{t=0}^{T-1} -\eta_t \rho \mu \mathbb{E}_{\sim \xi_t} [\|\nabla f(\mathbf{x}_t)\|^2] + \right. \\
&\quad \left. \frac{\eta_t^2 L}{2} \left(\mathbb{E}_{\sim \xi_t} [\|\nabla f(\mathbf{x}_t)\|^2] + \sigma^2 \right) \right) + C = \\
&\quad \left(\sum_{t=0}^{T-1} \left(-\eta_t \rho \mu + \frac{\eta_t^2 L}{2} \right) \mathbb{E}_{\sim \xi_t} [\|\nabla f(\mathbf{x}_t)\|^2] + \frac{\eta_t^2 L}{2} \sigma^2 \right) + C,
\end{aligned}$$

where for the second inequality we used the result of Appendix A.4.

We further manipulate the result by noticing that: $\sum_{t=0}^{T-1} \Delta_t = \mathbb{E}_\Omega [f(\mathbf{x}_{T+1}) - f(\mathbf{x}_0)]$. Moreover since $\Lambda = \mathbb{E}_\Omega [f(\mathbf{x}_0)] - \inf_{\mathbf{x}} f(\mathbf{x})$, it is easy to show that $\Lambda \geq \mathbb{E}_\Omega [f(\mathbf{x}_0) - f(\mathbf{x}_{T+1})] = -\sum_{t=0}^{T-1} \Delta_t$. We combine the bounds together as:

$$\begin{aligned}
-\Lambda &\leq \sum_{t=0}^{T-1} \Delta_t \leq \left(\sum_{t=0}^{T-1} \left(-\eta_t \rho \mu + \frac{\eta_t^2 L}{2} \right) \mathbb{E}_{\sim \xi_t} [\|\nabla f(\mathbf{x}_t)\|^2] \right. \\
&\quad \left. + \frac{\eta_t^2 L}{2} \sigma^2 \right) + C.
\end{aligned}$$

Then:

$$\begin{aligned}
-\Lambda - C &\leq \left(\sum_{t=0}^{T-1} \left(-\eta_t \rho \mu + \frac{\eta_t^2 L}{2} \right) \mathbb{E}_{\sim \xi_t} [\|\nabla f(\mathbf{x}_t)\|^2] \right. \\
&\quad \left. + \frac{\eta_t^2 L}{2} \sigma^2 \right),
\end{aligned}$$

and finally:

$$\begin{aligned}
&\left(\sum_{t=0}^{T-1} \left(\eta_t \rho \mu - \frac{\eta_t^2 L}{2} \right) \mathbb{E} [\|\nabla f(\mathbf{x}_t)\|^2] \right) \\
&\leq \left(\sum_{t=0}^{T-1} \left(\frac{\eta_t^2 L}{2} \sigma^2 \right) \right) + \Lambda + C.
\end{aligned}$$

We conclude that:

$$\min_{0 \leq t \leq T} \mathbb{E} [\|\nabla f(\mathbf{x}_t)\|^2] \leq \frac{\left(\sum_{t=0}^{T-1} \left(\frac{\eta_t^2 L}{2} \sigma^2 \right) \right) + \Lambda + C}{\sum_{t=0}^{T-1} \left(\eta_t \rho \mu - \frac{\eta_t^2 L}{2} \right)}.$$

We then proceed by proving the simple corollary 1 of Theorem 1. By choosing a suitable constant learning rate $\eta_t = \eta = \frac{\rho\mu}{L\sqrt{T}}$ we can rewrite the inequality as

$$\min_{0 \leq t \leq T} \mathbb{E} \left[\|\nabla f(\mathbf{x}_t)\|^2 \right] \leq \frac{\left(T \left(\frac{\eta^2 L}{2} \sigma^2 \right) \right) + \Lambda'}{T \left(\eta \rho \mu - \frac{\eta^2 L}{2} \right)}.$$

where for simplicity we have defined $\Lambda' = \Lambda + C$.

We then notice that $\eta \rho \mu = \frac{(\rho\mu)^2}{L\sqrt{T}}$ and that $\frac{\eta^2 L}{2} = \frac{(\rho\mu)^2}{2LT}$, consequently we can rewrite the upper bound as

$$\frac{\frac{(\rho\mu)^2 \sigma^2}{2L} + \Lambda'}{\frac{(\rho\mu)^2 \sqrt{T}}{L} - \frac{(\rho\mu)^2}{2L}} = \frac{\frac{(\rho\mu)^2 \sigma^2}{2L} + \Lambda'}{\frac{(\rho\mu)^2}{L} \left(\sqrt{T} - \frac{1}{2} \right)}.$$

Since we are interested in \mathcal{O} convergence rate, we can safely assume that $\left(\sqrt{T} - \frac{1}{2} \right) \simeq \sqrt{T}$ and that thus

$$\begin{aligned} \min_{0 \leq t \leq T} \mathbb{E} \left[\|\nabla f(\mathbf{x}_t)\|^2 \right] &\lesssim \frac{\frac{(\rho\mu)^2 \sigma^2}{2L} + \Lambda'}{\frac{(\rho\mu)^2}{L} \sqrt{T}} \\ &= \left(\frac{\sigma^2}{2} + \frac{\Lambda' L}{(\rho\mu)^2} \right) \frac{1}{\sqrt{T}} \end{aligned}$$

B The simulator and a note on staleness

In this Section we provide additional details to clarify the simulator structure, the definition of staleness and its generating process in our empirical validation. Figure 6 is an abstract representation of the distributed architecture we consider in this work. It consists of a time-line for each machine in the system: one for the *parameter server* (PS), and one for each worker W_i ($i = 3$ in the Figure).

In our system model, the PS accepts contributions from workers and updates the current model iterate according to the variant of the SGD algorithm it implements. We use the notation $\mathbf{x}_n = U(\mathbf{x}_{n-1}, \nabla(\mathbf{x}_k))$ to indicate that the n_{th} model version at PS is obtained by updating the $n - 1_{th}$ version using a gradient computed with the k_{th} version, according to the rules of the generic update algorithm $U(\cdot)$. In this case the staleness of the model update is equal to $n - 1 - k$. It is assumed that as soon as the PS update the parameters the worker immediately receives the updated model, indicated with $W_i \leftarrow \mathbf{x}_n$. Each worker is going to transmit many different updates ($N_{updates}$), each of which will reach the PS after a random delay. We define the sequence of delays for the i_{th} worker as $\{t_{\text{COMM},r}^{(i)}\}_{r=0}^{N_{updates}}$. The random generation process will be shortly after explained.

We are then ready to explain the example depicted in Figure 6:

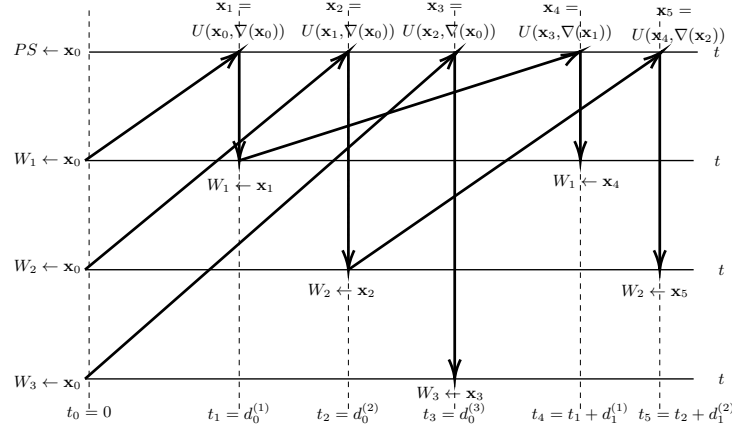


Fig. 6: Illustration of the distributed system operation. Example with one PS and 3 workers.

1. At time instant $t_0 = 0$ all workers and PS are initialized with model \mathbf{x}_0 .
2. At $t_1 = t_{\text{COMM},0}^{(1)}$ the PS receives the first gradient computed by W_1 using model \mathbf{x}_0 . The PS updates the model ($\mathbf{x}_1 = U(\mathbf{x}_0, \nabla(\mathbf{x}_0))$) and send the update to W_1 . In this case the staleness of the update is 0
3. At $t_2 = t_{\text{COMM},0}^{(2)}$ the PS receives the first gradient computed by W_2 using model \mathbf{x}_0 . The PS updates the model ($\mathbf{x}_2 = U(\mathbf{x}_1, \nabla(\mathbf{x}_0))$) and send the update to W_2 . In this case the staleness is $1 - 0 = 1$.
4. At $t_3 = t_{\text{COMM},0}^{(3)}$ the PS receives the first gradient computed by W_3 using model \mathbf{x}_0 . The PS updates the model ($\mathbf{x}_3 = U(\mathbf{x}_2, \nabla(\mathbf{x}_0))$) and send the update to W_3 . In this case the staleness is $3 - 1 = 2$.
5. At $t_4 = t_1 + t_{\text{COMM},1}^{(1)}$ the PS receives the second gradient computed by W_1 using model \mathbf{x}_1 . The PS updates the model ($\mathbf{x}_4 = U(\mathbf{x}_3, \nabla(\mathbf{x}_1))$) and send the update to W_1 . In this case the staleness is $2 - 0 = 2$.
6. At $t_5 = t_2 + t_{\text{COMM},1}^{(2)}$ the PS receives the second gradient computed by W_2 using model \mathbf{x}_2 . The PS updates the model ($\mathbf{x}_5 = U(\mathbf{x}_4, \nabla(\mathbf{x}_2))$) and send the update to W_2 . In this case the staleness is $4 - 2 = 2$.
7. ...

Each communication delay is generated according to an exponential probability distribution with rate λ . To simulate network heterogeneity each worker has its own (fixed throughout the simulation) rate λ_i . These rates are extracted independently for each worker according to a lognormal distribution, i.e. $\ln(\lambda_i) \sim \mathcal{N}(0, \sigma^2)$ where σ^2 is a user defined parameter that can be used to change statistical configurations of the system. We use Figure 7 to illustrate the delay distribution for an entire simulation, that is, from the first model iterate, until the end of the training phase. Every time the PS receives a contribution from a worker, it increments the count in the bin corresponding to the staleness of the stochastic gradient message. In the Figure we vary σ^2 to obtain different delay

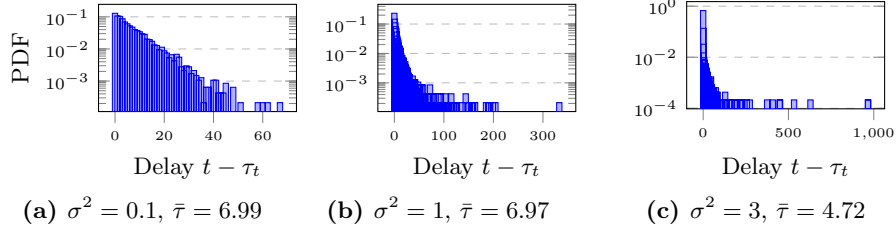


Fig. 7: Delay distributions of a simulation run with LENET on MNIST, in a distributed setting with 8 workers. For each worker we generate a network delay according to an exponential distribution with rate λ . We sample λ from a log-normal distribution with mean 0 and variance σ^2 . For each configuration, we also report the resulting average staleness $\bar{\tau}$.

distributions. Using a larger variance induces very large delay values (long tail in the distribution). However, if we observe the average staleness $\bar{\tau}$, we notice it decreases, because the mass of the distribution is concentrated on the left, which in practice means the majority of workers experience small delays.

From an implementation point of view, our work is divided in two tasks: the simulation of the delays and the simulation of the distributed architecture. The delays simulation is simply a generation of a sequence of random variables according to a given distribution, while to simulate the distributed system it is sufficient allocate in memory $N_{worker} + 1$ versions of the model (workers and PS) and update them according to the order of arrival of messages. It is important to notice that the simulator is transparent to the underlying mechanisms for computing gradients and updates. In this work, we use the PYTORCH-1.4 library to describe models, and how they are trained. The interface between the high and low level layers allows exchanging model iterates, and gradients. Note that we use automatic differentiation from PYTORCH-1.4 to compute gradients.

Overall, the above software design allows to: 1) easily introduce new models to study, as they can be readily imported from legacy PYTORCH-1.4 code; 2) easily implement variants of stochastic optimization algorithms; 3) experiment with a variety of system configurations, including heterogeneity, various communication patterns, and various staleness distributions.

C Train loss results

D Detailed experimental settings

General parameters

- Number of simulation runs per experimental setting: 5, with best parameters
- Number of workers = $\{1, 2, 4, 8, 16, 32, 64, 128\}$
- $t_{\text{COMM}} \sim \text{Exp}(\lambda)$
- $\ln(\lambda) \sim \mathcal{N}(0, \sigma^2)$, $\sigma^2 = \{0.1, 1, 3\}$

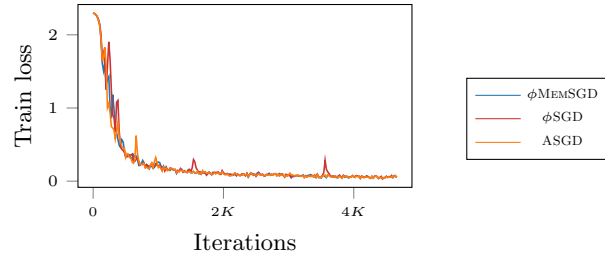


Fig. 8: Train loss for LENET on MNIST, in a system with 8 workers and $\sigma^2 = 0.1$

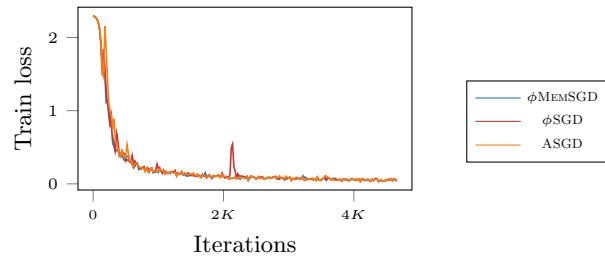


Fig. 9: Train loss for LENET on MNIST, in a system with 8 workers and $\sigma^2 = 1.0$

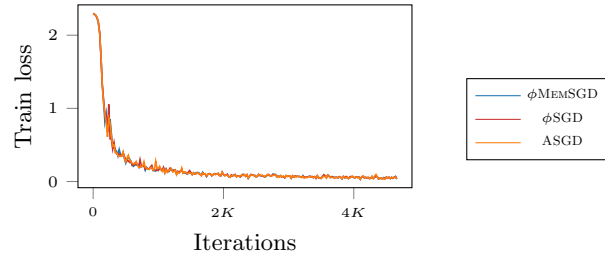


Fig. 10: Train loss for LENET on MNIST, in a system with 8 workers and $\sigma^2 = 3.0$

η	ϕMEMSGD	ϕMEMSGD	ASGD
LENET	0.01	0.01	0.01
RESNET-56	0.1	0.1	0.1
RESNET-56 - 32 workers	0.005	0.005	0.005

Table 2: Learning rate parameters.

Models. All model parameters we used, including learning rates and momentum, are specified in Table 2 and Table 3. Additional details are as follows.

- Training epochs = 5 (LENET), 161 (RESNET-56)

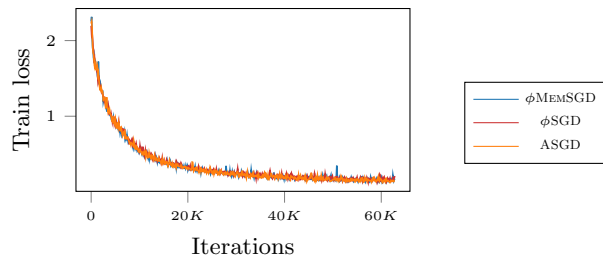


Fig. 11: Train loss for RESNET-56 on CIFAR10, in a system with 8 workers and $\sigma^2 = 0.1$

momentum	ϕ MEMSGD	ϕ MEMSGD	ASGD
LENET	0.5	0.5	0.5
RESNET-56	0.9	0.9	0.9

Table 3: Momentum parameters.

- Training mini-batch size = 64 (LENET), 128 (RESNET-56)
- Testing mini-batch size = 64 (LENET), 128 (RESNET-56)

The CNN models are implemented in PYTORCH-1.X.

- LE NET: architecture, $d = 61706$
- RESNET-56: architecture, $d = 590426$